Testing the Probability of Clear Line of Sight Models with ARM Observations

Y. Ma
Department of Meteorology
University of Maryland
College Park, Maryland

R. G. Ellingson
Department of Meteorology
Florida State University
Tallahassee, Florida

Abstract

Clouds play a major role in regulating Earth's climate. However, computer models of Earth's climate neglect the effects of cloud vertical extend in a broken cloud field. The vertical extent allows clouds to shade more of the atmosphere and allow radiative exchange over a larger temperature range. One way to parameterize this 3D cloud effect is to relate the various cloud properties, including the cloud vertical extent, to a statistical cloud field parameter called the probability of clear line of sight (PCLS) (see Figure 1) and then to a simple integral parameter – the effective-cloud-fraction (N_e). PCLS is a summary description of the geometric distribution of a cloud field. It depends on the cloud location, cloud size, and cloud shape. Given different probability distributions for the location, size, and shape, we may format different PCLS models. We are trying to test various PCLS models with Atmospheric Radiation Measurement (ARM) cloud observations. In order to achieve this, we need to infer such cloud properties as the absolute N (N), cloud thickness, cloud spacing, and horizontal size, from various ARM observations, including, the total sky imager (TSI), the whole sky imager (WSI), the narrow field of view sensor (NFOV), the millimeter-wave cloud radar (MMCR), and several Lidar instruments. In this paper, the cloud properties over the ARM Cloud and Radiation Testbed (CART) site during the spring and summer seasons of the 2000 and 2001 will be shown. Various PCLS models will be tested against observed PCLS values.

Longwave Flux Calculations under Broken Clouds

In climate studies, the longwave radiative fluxes are usually calculated as the cloud amount (N) weighted average of the values for homogeneous clear and cloudy sky conditions. N is usually assumed the fractional coverage of the vertical projections of plane-parallel clouds. However, under broken cloud conditions, cloud vertical extent will also contribute considerable amount of coverage. To keep this computer-time-saving method but also account for the finite size effects of the clouds in the calculation of the longwave radiation, one may define an N_e, such that

$$F = (1 - N_e)\, F_{clear} + N_e\, F_{overcast}.$$

F - downwelling flux of radiant energy at the surface; subscripts clear and overcast denote fluxes for those conditions

N_e - effective N

= function of the absolute N, droplet radii, water phase, distribution of cloud centers, size distribution, cloud shape…, depending upon the complexity of the cloud model.

The effective N is the plane-parallel N that generates the same flux as the detailed models for a given broken cloud field after taking into account the effects of geometric shapes, size, spatial distribution, and absolute amount (N) of clouds. These effects may be integrated into N_e through a single cloud field property – the PCLS.

The Probability of a Clear Line of Sight

PCLS is a function of the geometric properties of the cloud field. Such properties include: (1) the shape and size of the cloud domain; (2) the cloud center distribution; (3) the cloud size distribution; and (4) the shape of the clouds. Different methods of specifying these properties will lead to different PCLS models. For example, if we assume the clouds have identical base heights, are randomly distributed in an infinitely large horizontal plane, and are right cylinders or semi-ellipsoids, then we can model the PCLS at zenith angle θ as

$$p(\theta) = (1\text{-}N)^{f(\theta)}, \text{ where } f(\theta) = \begin{cases} 1 + 4\beta \tan\theta, & \text{for Right} - \text{cylinder} \\ \frac{1}{2}\left(\frac{\pi}{\sqrt{1 + 4\beta^2 \tan^2\theta + 1}}\right), & \text{for Semi} - \text{ellipsoid} \end{cases}$$

where β is the cloud aspect ratio defined as the ratio of the cloud height to the horizontal size. Figure 1 shows several example PCLS's using the above model. The PCLS monotonously decreases from (1-N) at zenith to zero at the horizon. For the above model, we may also notice that the cloud shape has considerable effect on the PCLS. The PCLS difference between right-cylinder and semi-ellipsoid is equivalent to the change in β from 0.5 to 1.0.

Inferring Cloud Parameters from ARM-CART Observations

To achieve our objective of testing the various PCLS models, we need to obtain the cloud field properties such as the horizontal size, the absolute N, the vertical thickness of the clouds and the PCLS.

Cloud Spacing and Horizontal Size

Assuming that the cloud field properties do not change significantly as they move past at the mean wind speed (the frozen turbulence hypothesis), the spacing and horizontal sizes are estimated as the products of the wind speed and the lengths of the time intervals from a time series of observations of the cloud field. The wind speed at cloud height is determined from the 915 MHz radar wind profiler (RWP915) data. The NFOV data is used to infer the spacing and cloud time interval lengths. The output of the

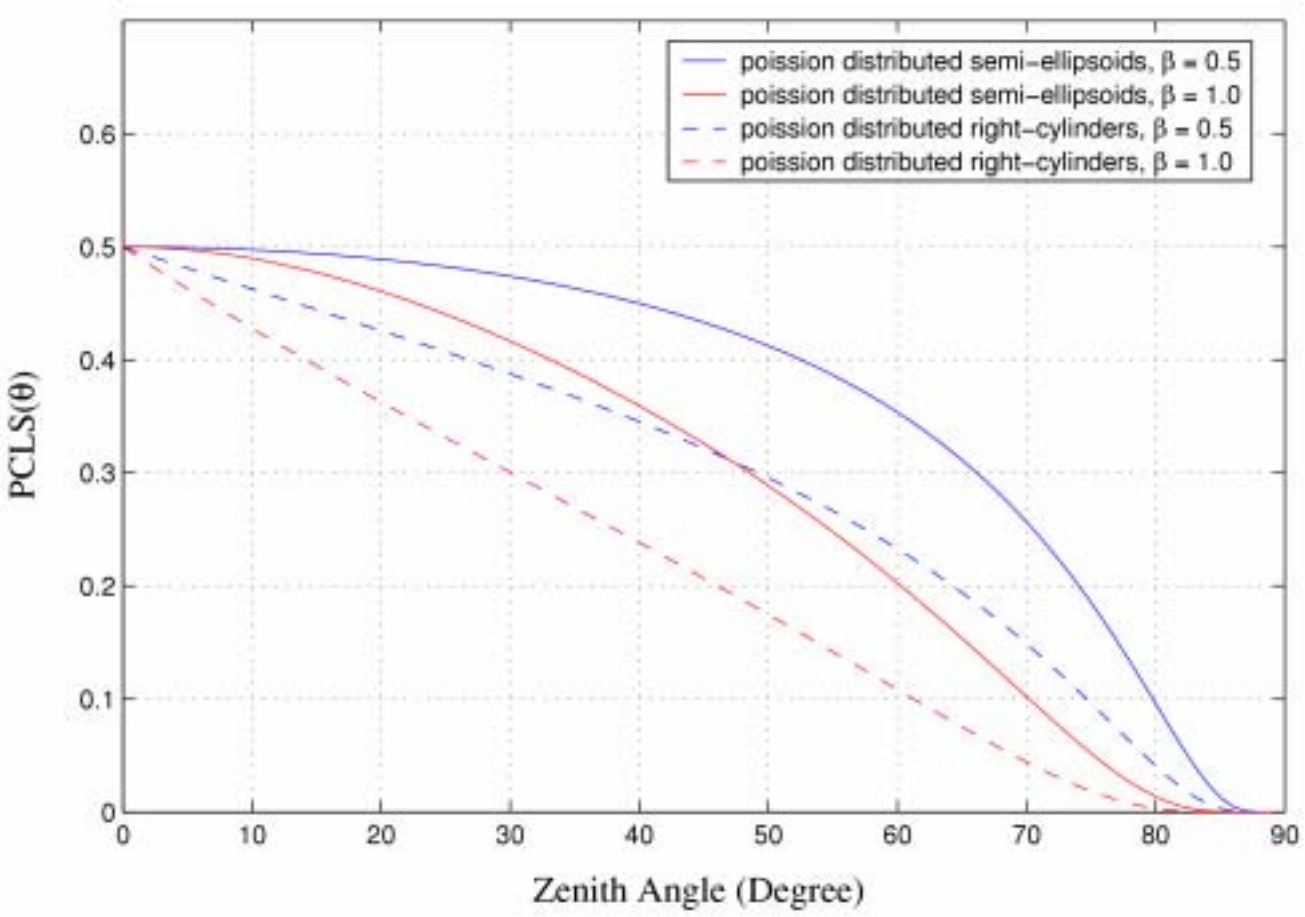

Figure 1. PCLS for Poission distributed clouds.

NFOV consists of a time series of 1-sec observations of the zenith spectral radiance at wavelength of 869 nm (see Figure 2b), where the red line is a threshold to classify the cloud and clear-sky. Figure 2a shows the distributions of the inferred cloud spacing and horizontal sizes for all of the cases obtained. The stair step line is the histogram of the spacings and sizes. Since we used a set of non-uniform-width bins, the ordinate values of the histogram have been scaled to the number of counts per unit length (= #counts within a bin / bin width). The fitted Weibull distributions works well for the lower end of the spacings and the sizes, but tend to underestimate the larger spacings and sizes. The straight line is the fitted power law distributions.

Absolute Cloud Fraction

The absolute cloud amount is defined as the fractional area of the vertical projections of the clouds on the surface. Without large area imagery data over the ARM-CART site, we inferred the absolute amount by using the same assumptions as for cloud spacing, and estimated N = l/L, where L is the total length of a time series of observation and l is the length of the cloud segments.

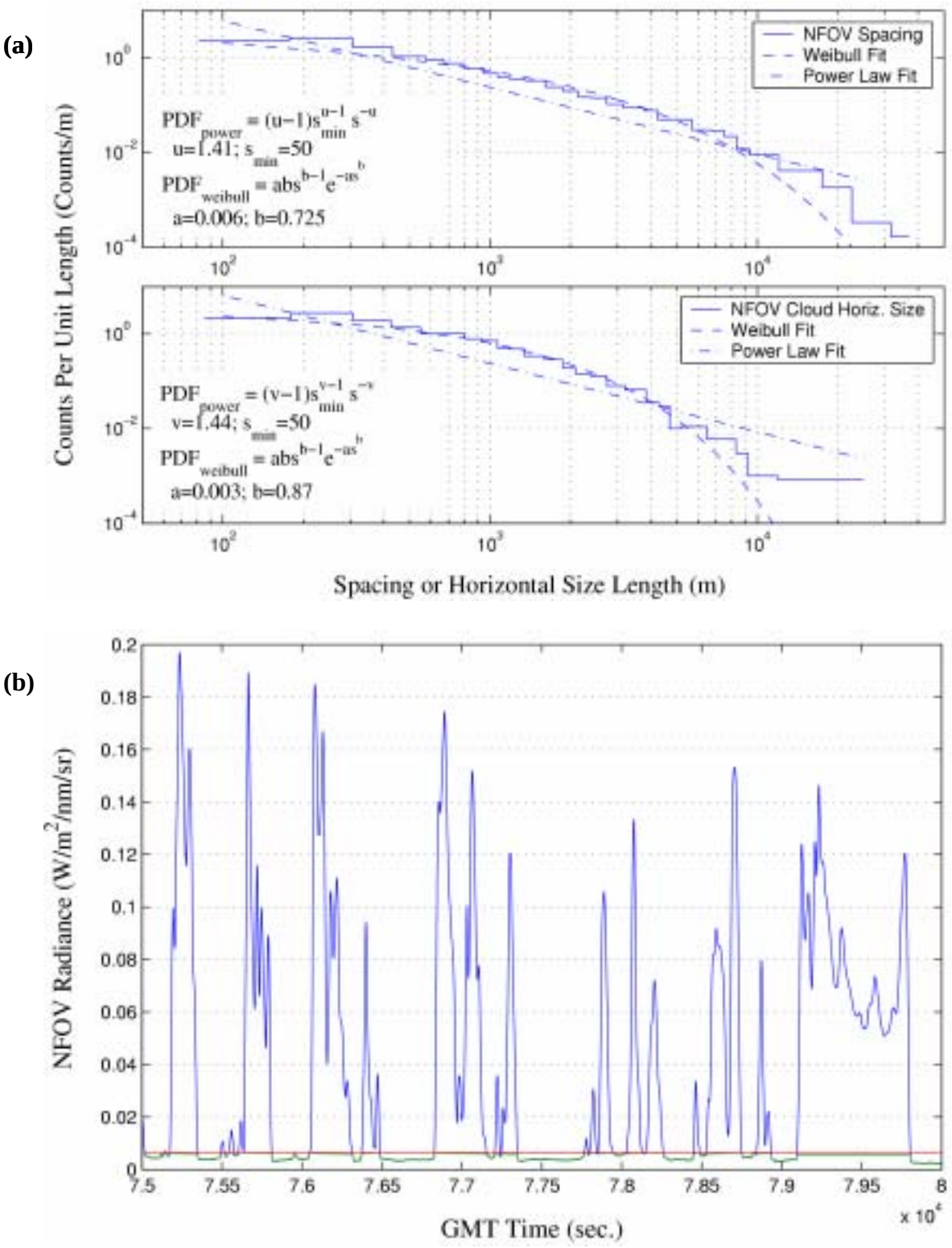

Figure 2. (a) Cloud spacing and horizontal size distributions from the NFOV. (b) A time series of the downwelling zenith radiance from the NFOV.

Three instruments, the NFOV, TSI, and the WSI, have been used to obtain the N. When using the TSI and the WSI, the image sequence of the central circle of a field-of-view of 20° is used to calculate the N. Figure 3 gives the comparison of the three N's. The N_{WSI} agree well with the N_{TSI} but with a little larger variance, while the N_{NFOV} tend to overestimate the cloud amount. This is probably because the WSI has a lower sampling frequency than TSI, while the NFOV is too sensitive to small and thin clouds.

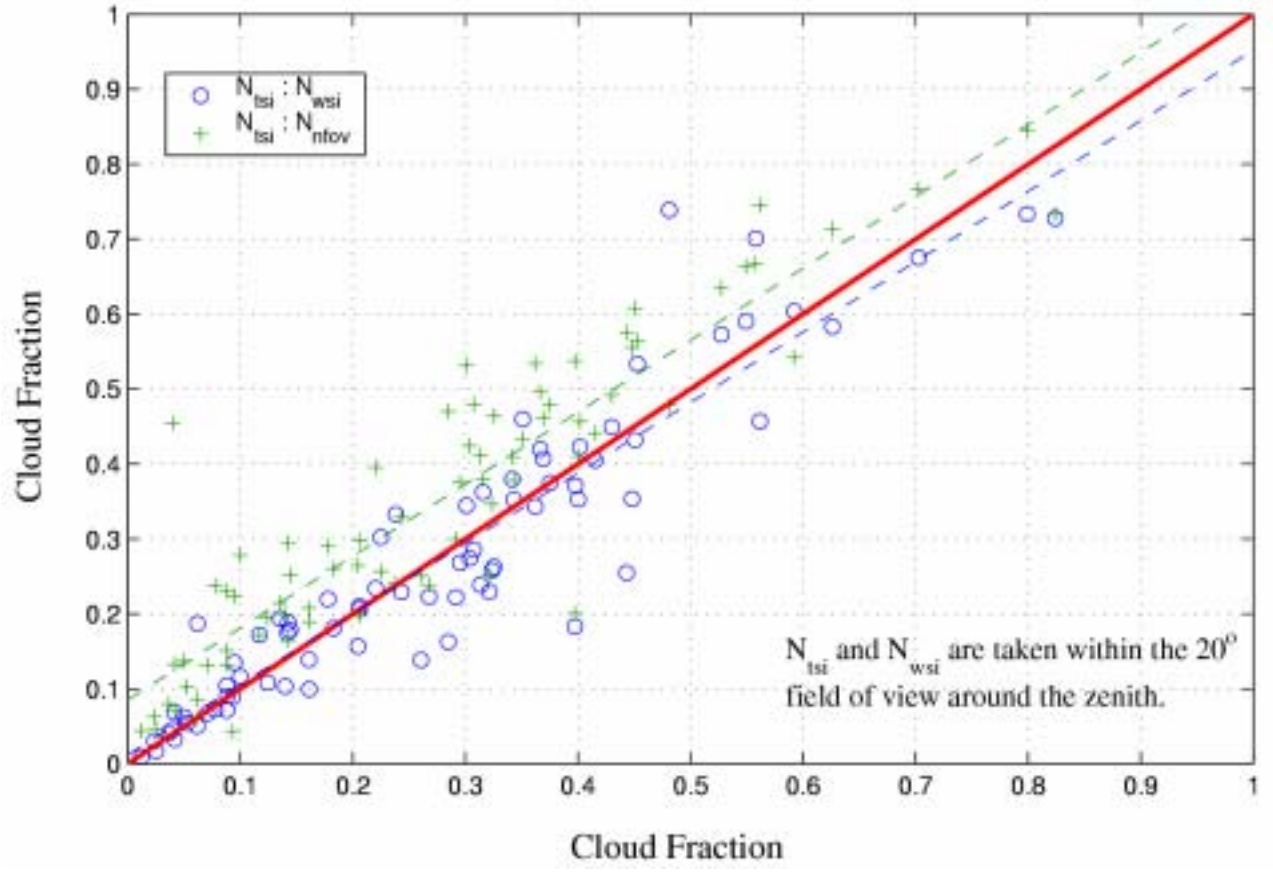

Figure 3. Absolute cloud amount from the TSI, WSI, and the NFOV.

The PCLS

The PCLS is estimated from the WSI and TSI data. Since the WSI and the TSI instantaneously measure the presence or absence of clouds at a given zenith and azimuth angle, time and azimuth averages of the data yield an approximation to PCLS(θ). The ergotic assumption allows the extension to a spatial average. In this study estimates of the fraction of clear pixels within each 1° annular ring from zenith to instrument horizon were determined for each image on a day when only cumulus clouds ere present. PCLS(θ) is determined by averaging over several images. Figures 4a and b are two classified cloud images from the WSI and TSI, respectively, taken at 22:18:00GMT, July 22, 2000.

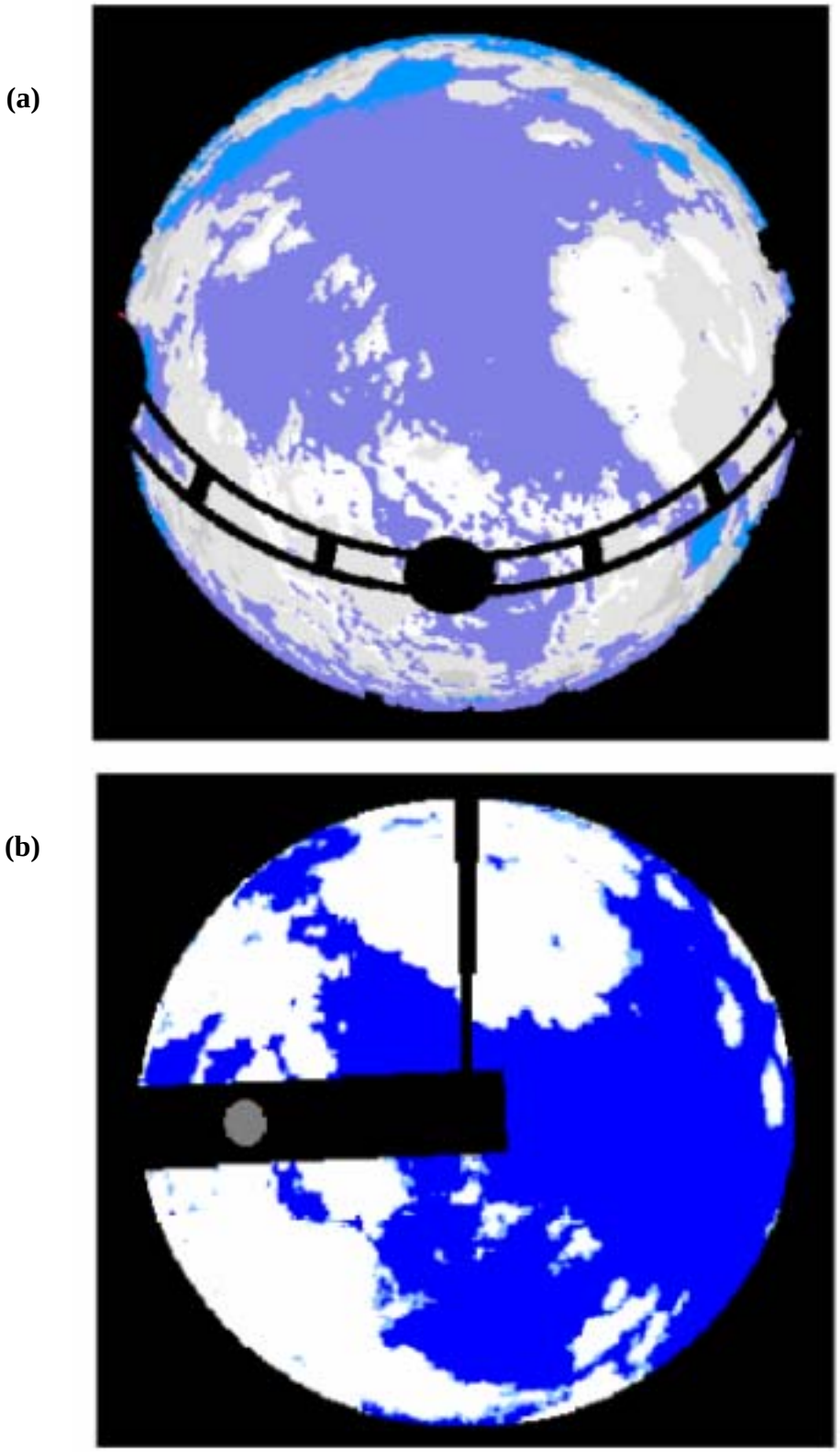

Figure 4. Cloud images from the (a) WSI and (b) TSI at 22:18:00 GMT, July, 22, 2000.

Figure 5 shows the difference between the PCLS estimated from the WSI and the TSI obtained as an average of 93 cases of single layer fair weather cumulus cloud fields measured over the ARM-CART site during spring and summer seasons of 2000 and 2001. From the figure, we notice that below 60° the $PCLS_{WSI}$ agree well with the $PCLS_{TSI}$ with a standard deviation of about 0.7. While above 60°, the WSI tend to give larger N (or less value of the PCLS).

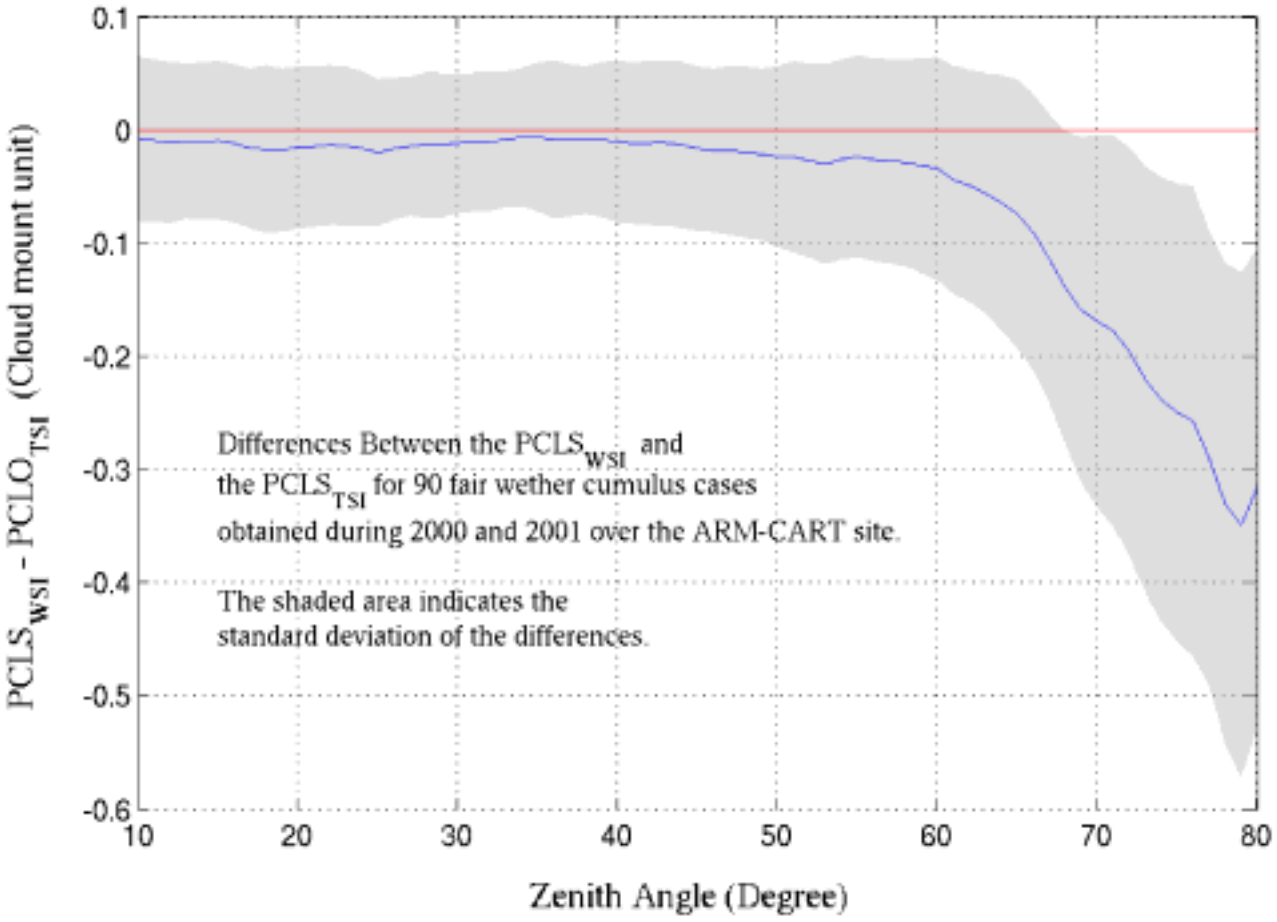

Figure 5. Differences between the PCLS values derived from the WSI and TSI.

Cloud Thickness

Several laser instruments at the ARM-CART site directly measure cloud base height. The ARSCL products give a good estimate of the cloud base height by merging these laser observations. Due to the clutter problem, it is sometimes difficult to determine the top height of the fair weather cumulus from the MMCR observations. In order to overcome this difficulty, we tried to combine information from the MMCR and the relative humidity (RH) profiles to infer the needed cloud top height. Figures 6 - 8 illustrate the process. First, we obtain an initial cloud top height from the ARSCL data. This top height is checked with the available RH profiles.

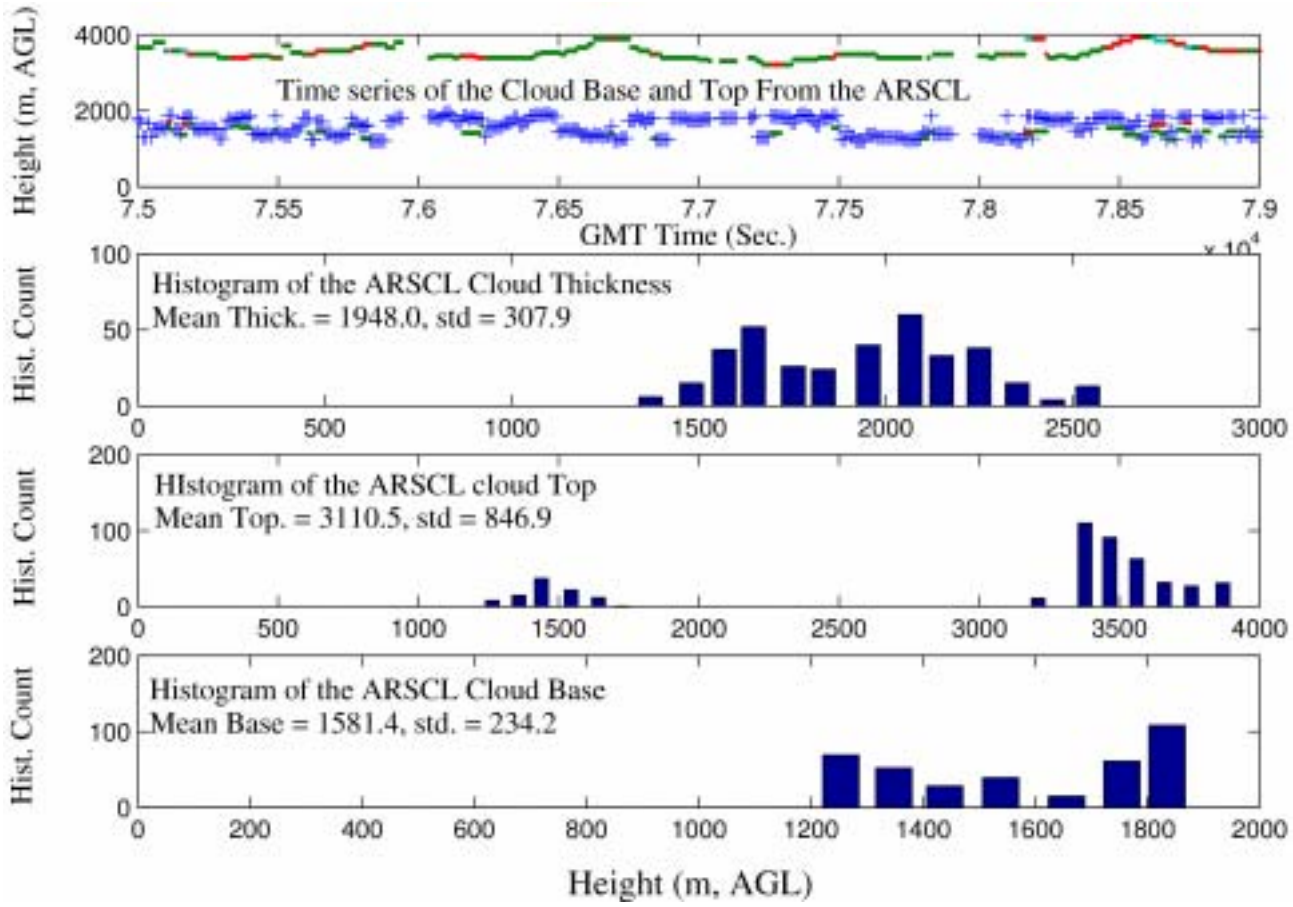

Figure 6. Inferring the cloud thickness from the ARSCL data.

If the RH profiles indicate a clear cloud top layer and this layer is much different from the MMCR measurement, then we take the RH height as the final cloud top height. Figure 6 is the process of estimation of the initial thickness using the ARSCL data. Figure 7 gives an example of the RH profile corresponding to the time of Figure 6. Figure 7 shows histograms of the obtained cloud thicknesses. The correction based on the RH profiles mainly eliminates some larger cloud thickness reported by the MMCR.

Comparison the Various PCLS Models with the TSI Observations

From spring and summer seasons of 2000 and 2001, 93 fair weather cumulus cases are selected to test the various PCLS models. For every case, model calculated PCLS is compared with the TSI observed PCLS. Figure 9 shows the averaged differences between the $PCLS_{model}$ and the $PCLS_{TSI}$. All the listed models agree with the observations within -0.15 to ~+0.1 (N unit). The Poisson distributed hemisphere, semi-ellipsoid or ellipsoid tend to give better agreement with the observations, especially within 60° around the zenith. Figure 10 shows the statistics of various model predictions of the cloud side effect and the one interred from the TSI observations. The cloud side effect is defined as

$$F = N_e - N, \text{ or for isothermal clouds } f = 2\int_0^1 [1 - N - P_{cir}(\mu)]udu$$

In the plot, the 7th column is f from the TSI, which indicates that for those fair weather cumulus over the ARM-CART site, the mean flux departure at the surface due to the cloud side effects is about 3W m^{-2} (assuming the cloud base is 2 km). Among the model predictions, we see that the randomly distributed hemispheres generated better results.

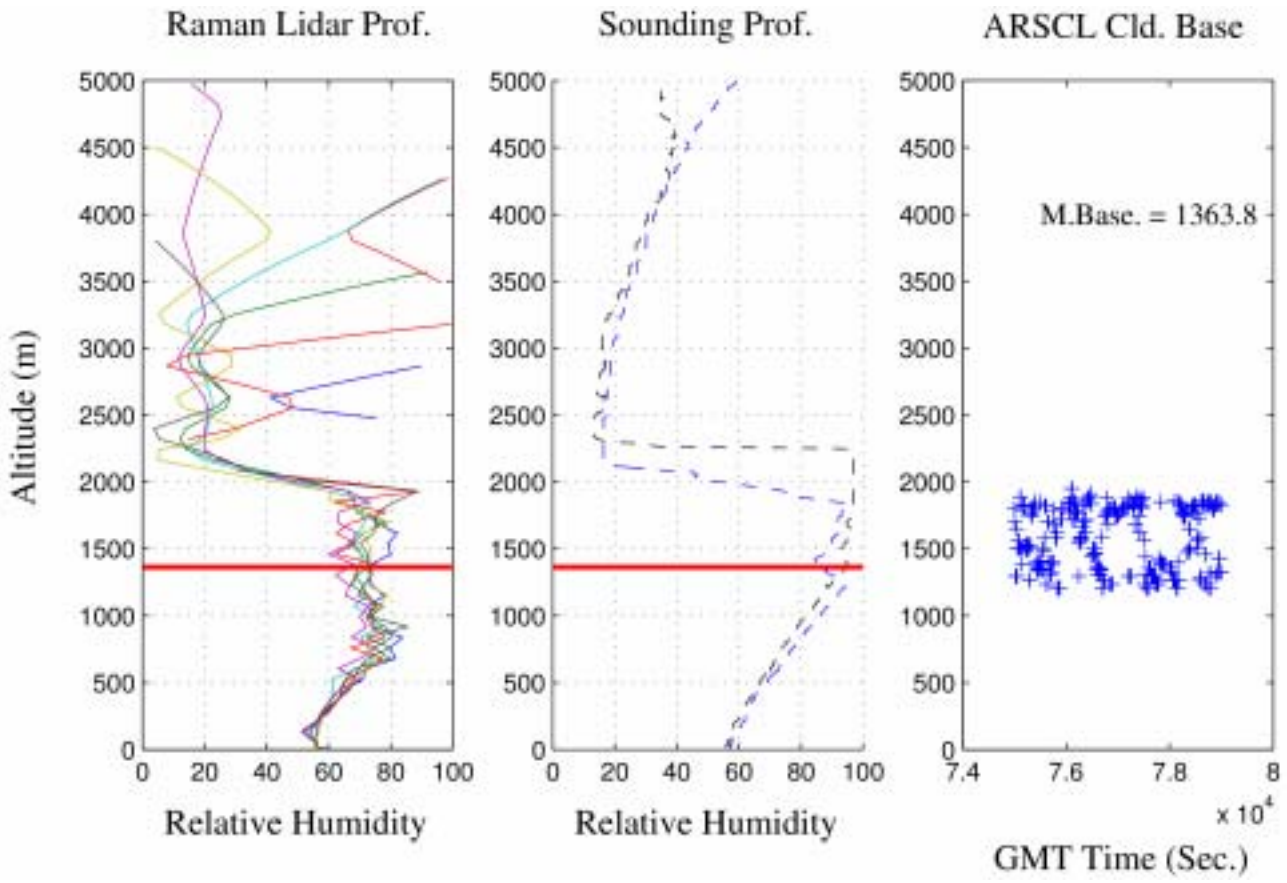

Figure 7. Estimating the cloud thickness from the RH profiles.

Conclusions

- For the longwave radiation under broken cloud conditions, the 3D cloud geometric effects can be parameterized by the use of a N_e that is a function of the PCLS. For black body clouds, the PCLS is a function of the cloud geometry and cloud spatial and size distributions. Given various combinations of the cloud geometry, spatial and size distributions, one may construct many different PCLS models

- Quantities needed to test various PCLS models are estimated by assuming the frozen turbulence approximation. The PCLS is estimated from the TSI images, the absolute cloud amount and the horizontal size are inferred from the NFOV and the TSI. The cloud thickness is obtained from combinational use of the ARSCL and the RH data.

- Various PCLS models are tested against the observations. For the fair weather cumulus over the ARM-CART sites, the randomly distributed hemisphere model tends to give better average results. Even for small cumulus (the fair weather cumulus) over the Southern Great Plains, the cloud side effects may generate a significant flux departure relative to the black plate approximation.

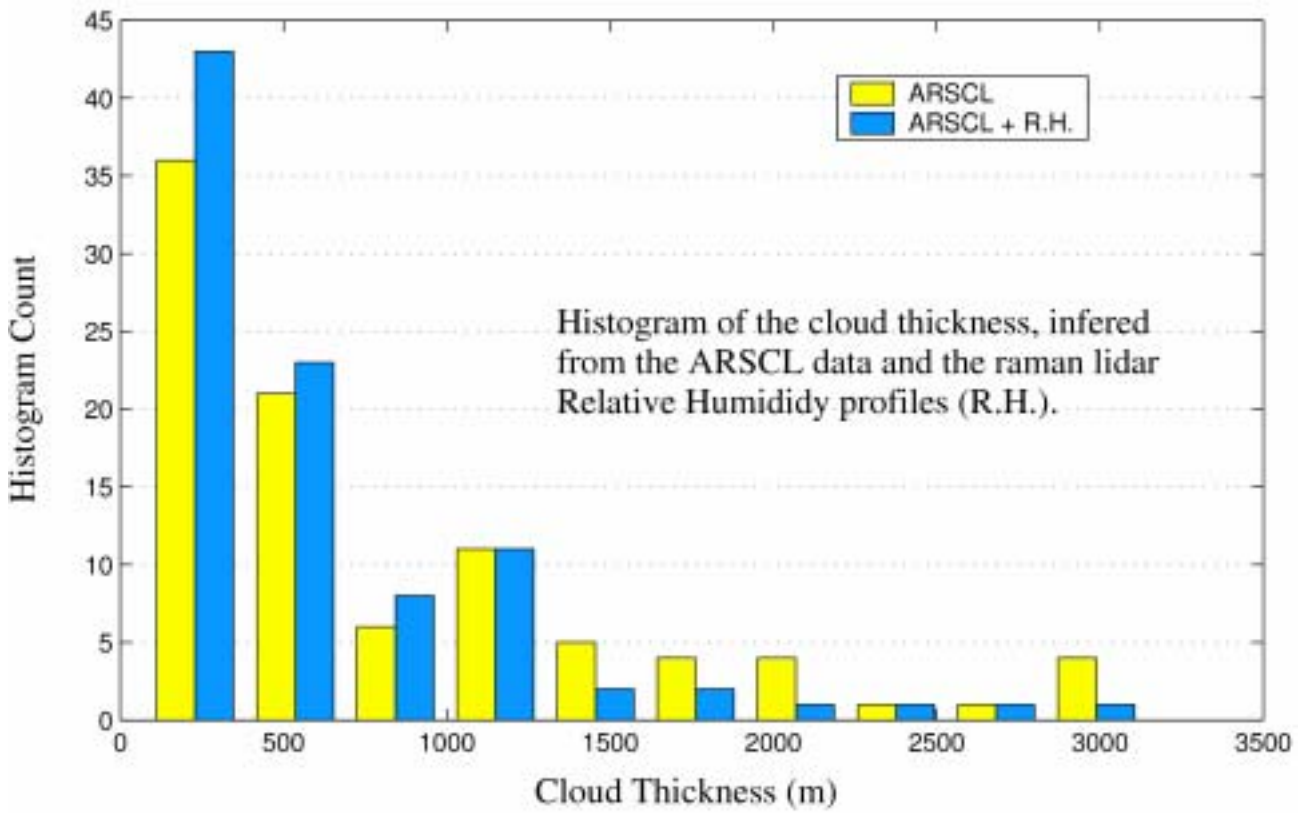

Figure 8. Cloud thickness for 90 cases of fair weather cumulus fields.

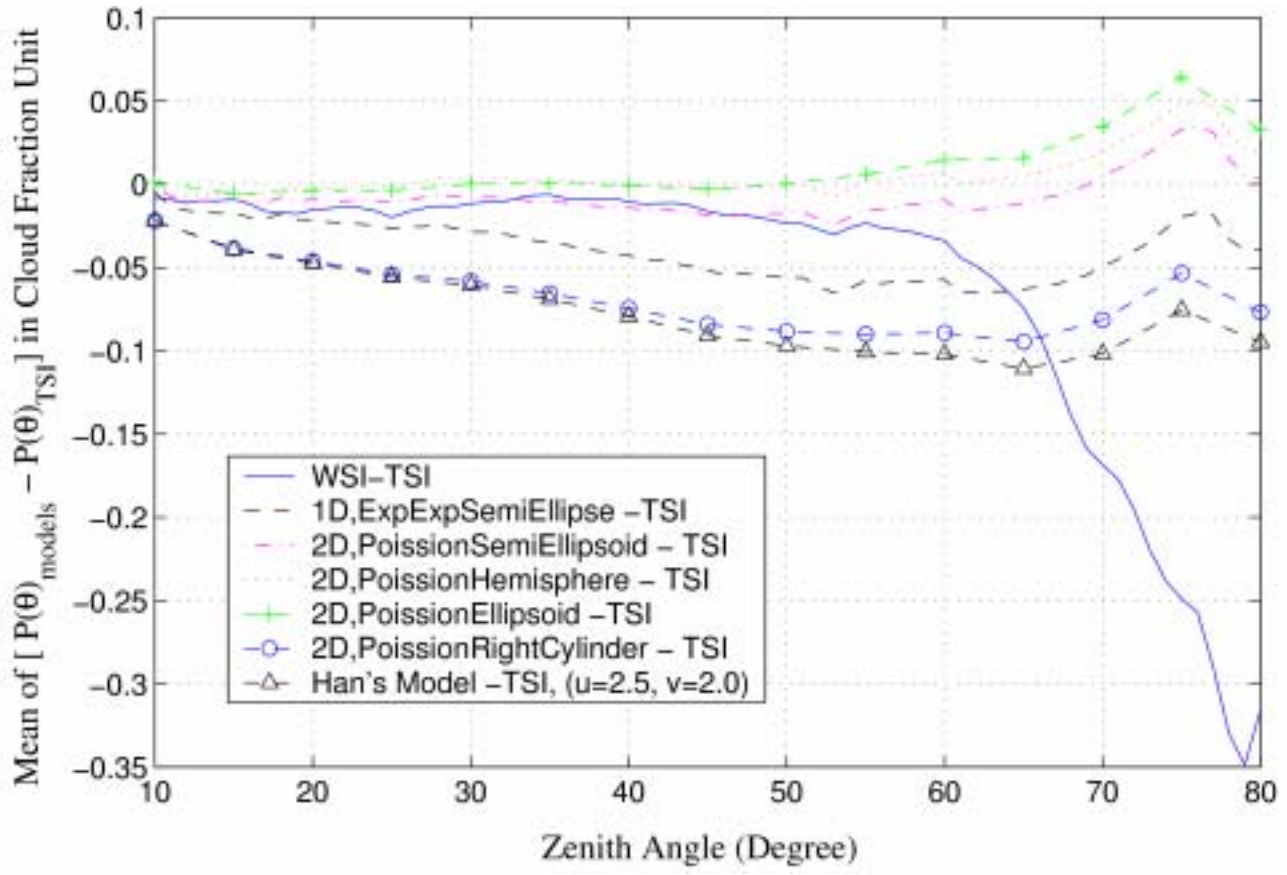

Figure 9. The mean values of [$P(\theta)_{models} - P(\theta)_{TSI}$]

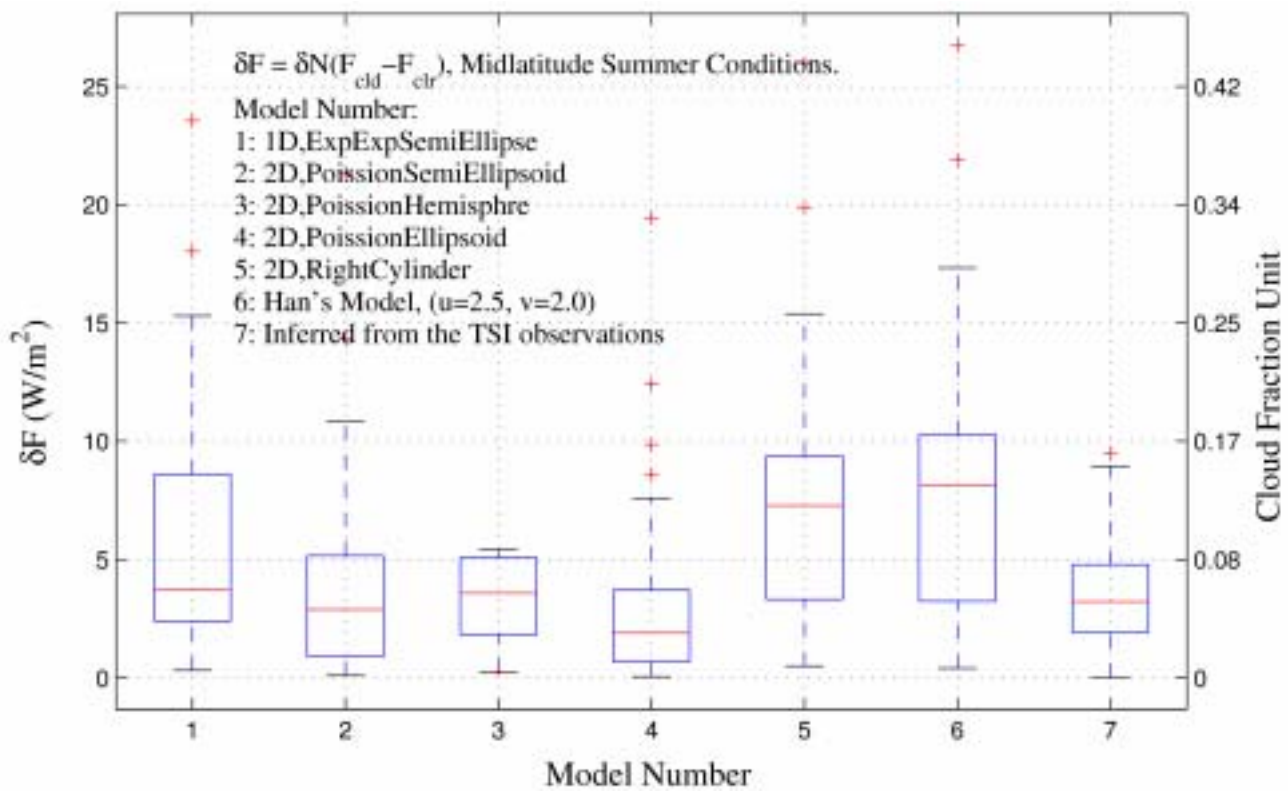

Figure 10. Cloud side effects from the models and the TSI observations for the fair weather cumulus fields.